Depletion kinetics of Mo(a7S3,a5S2,a5D J) by N2, SO2, CO2, N2O, and NO

ARTICLE *in* THE JOURNAL OF PHYSICAL CHEMISTRY · MAY 1996

Impact Factor: 2.78 · DOI: 10.1021/jp9532172

3 AUTHORS, INCLUDING:

Mark L. Campbell
United States Naval Academy
55 PUBLICATIONS **861** CITATIONS

SEE PROFILE

Depletion Kinetics of Mo(a^7S_3,a^5S_2,a^5D_J) by N_2, SO_2, CO_2, N_2O, and NO

Roy E. McClean,* Mark L. Campbell, and Robert H. Goodwin

Chemistry Department, United States Naval Academy, Annapolis, Maryland 21402

Received: October 31, 1995; In Final Form: January 30, 1996[⊗]

The gas phase collisional disappearance of Mo(a^7S_3,a^5S_2,a^5D_J) in the presence of N_2, SO_2, CO_2, N_2O, and NO over the temperature range 294−621 K and in the total pressure range 10−600 Torr is reported. Mo atoms were produced by the 248 nm photodissociation of $Mo(CO)_6$ and $MoCl_4$ and detected by laser-induced fluorescence. The room temperature depletion rate constant of Mo(a^5S_2) + N_2 is $(2.3 \pm 0.7) \times 10^{-11}$ cm^3 s^{-1}; the depletion rate constants of the a^5D_J are smaller and range from $(16 \pm 8) \times 10^{-12}$ for Mo(a^5D_0) to $(0.13 \pm 0.04) \times 10^{-12}$ cm^3 s^{-1} for the other spin−orbit states. The depletion rate of all states of Mo by SO_2 are on the order of the collision rate. Mo(a^7S_3) is found to be unreactive toward CO_2, and the rate constant for the reaction of Mo(a^7S_3) with N_2O is expressed as $k(T) = (2.0 \pm 0.5) \times 10^{-10} \exp[-(9.8 \pm 0.3)$ kcal mol$^{-1}/RT]$ cm^3 s^{-1}. Termolecular kinetics are observed for Mo(a^7S_3) + NO with $k_0 = (2.6 \pm 0.3) \times 10^{-29}$ cm^6 s^{-1}, $k_\infty = (5.8 \pm 0.5) \times 10^{-11}$ cm^3 s^{-1}, and $F_c = 0.72 \pm 0.07$ at 296 K; the reaction rates for this reaction decrease with increasing temperature. Depletion rate constants of the reactions of the excited states of Mo with CO_2, N_2O, and NO are on the order of 10^{-12}−10^{-10} cm^3 s^{-1}; the depletion kinetics are complex and involve significant energy transfers. Results indicate that the electron configuration of Mo plays a role in its depletion kinetics. In all cases, Mo($4d^55s^1a^5S_2$) depletes faster than Mo($4d^45s^2a^5D_J$). The inefficient reactions of Mo(a^7S_3) with CO_2 and N_2O are attributed to the production of spin-forbidden states.

Introduction

We recently reported an investigation of the reaction kinetics of Mo(a^7S_3,a^5S_2,a^5D_J,a^5G_J) with O_2.[1] That study was an effort to understand the dynamics of Mo oxidation reactions and to determine possible oxidation mechanisms of transition metal (TM) atoms. We found that the reaction kinetics of Mo with O_2 were independent of total pressure (Ar buffer), observations consistent with bimolecular reaction kinetics. The a^7S_3, a^5S_2, and a^5G_J states have measured rate constants on the order of the collision rate constant, and the a^5D_J spin−orbit states have smaller rate constants that are temperature dependent. Results were interpreted in terms of a direct abstraction mechanism.[1,2] In this mechanism, atomic states evolving from electron configurations that correlate to the product metal oxide states react faster than those atomic states that do not correlate with the product states. Reaction barriers are expected to arise along the surfaces for the states that do not correlate. In the Mo case, atomic states evolving from the $4d^55s^1$ configuration orbitally correlate with $2\delta^2 12\sigma^1 6\pi^1$ MoO($X^5\Pi_r$) and several low-energy molecular states.[3] The a^7S_3 (ground state), a^5S_2, and a^5G_J states have $4d^55s^1$ configurations, and the a^5D_J term has a $4d^45s^2$ configuration. The electron configurations and energies of the Mo states studied here are summarized in Table 1.[4,5] The a^5G_J term, which is not shown in Table 1, has as its lowest energy 16 641.08 cm^{-1}.

We extend the Mo + O_2 study to an investigation of the reactivity of Mo(a^7S_3,a^5S_2,a^5D_J) with SO_2, CO_2, N_2O, and NO. SO_2, CO_2, and N_2O are closed-shell molecules while NO is a stable radical. There is a reasonable range of electron affinities among these reactants and O_2 such that the reactivity of different electronic states of Mo toward different types of oxygen-containing molecules can be assessed and the driving force for reaction can be ascertained. The electron affinity, EA, is an important quantity in the electron-transfer mechanism, a short-range version of the harpoon mechanism used to explain the large reaction cross sections of metal atoms with oxidants.[2,6] The potential energy surfaces deriving from the reactant states cross an ion-pair surface in this mechanism. Depletion efficiencies thus depend on the electron affinity of the oxidant, OX, and on the ionization potential, IP, of the TM atom. The electron-transfer mechanism has been applied to reactions involving main group metal atoms as well as TM atoms. A semiempirical, resonance interaction model has also been developed to explain reactions of metal atoms with N_2O.[7] This model predicts activation energies and correlates rate constants and activation energies to the sum of IPs and s−p promotion energies, PE. We compare the *depletion* kinetics of Mo states with respect to electron configurations and test the models above with our data.

TABLE 1: Electronic Configurations and LIF Excitation Information[a]

state	electronic config	energy (cm^{-1})	wavelength (nm)	detection filter (nm)[b]
a^7S_3	$4d^55s^1$	0	386.41	400
			390.30	390[c]
a^5S_2	$4d^55s^1$	10 768.33	550.65	600
a^5D_0	$4d^45s^2$	10 965.97	379.73	600
a^5D_1	$4d^45s^2$	11 142.83	384.72	600
a^5D_2	$4d^45s^2$	11 454.42	579.19	550
a^5D_3	$4d^45s^2$	11 858.54	388.68	600
a^5D_4	$4d^45s^2$	12 346.31	603.07	550

[a] References 4 and 5. [b] Broad-band filter with fwhm = 50 nm. [c] Narrow-band filter with fwhm = 10 nm.

The reactions of Mo(a^7S_3) with O_2, CO_2, N_2O, and NO have been observed in a shock tube apparatus at temperatures greater than ≈1200 K,[8] and a room temperature flow tube study of the reactivity of Mo(a^7S_3) with O_2, CO_2, and N_2O has recently been reported.[9] We are unaware of any other studies on the reactions reported here.

[⊗] Abstract published in *Advance ACS Abstracts,* April 1, 1996.

S0022-3654(95)03217-5

Experimental Section

Experiments were carried out in a slowly flowing apparatus using a laser photolysis/laser-induced fluorescence (LIF) technique. Reactions of Mo + oxidant were studied under pseudo-first-order conditions where the pressure of the oxidant greatly exceeded the pressure of the Mo precursor (and hence, Mo). Details of the experiment have been described elsewhere[1,2] and are only summarized here. The reaction chamber was a stainless steel cross that was contained in a convection oven. Molybdenum atoms were produced by the 248 nm photodissociation of $Mo(CO)_6$ or $MoCl_4$ with the unfocused output of an excimer laser operating at 15 Hz. Photolysis laser fluences inside the chamber were ≈60 mJ/cm^2, although fluences were varied over a factor of ≈5 to study their effects on thermalization and reaction rates. Molybdenum atoms were detected via LIF using laser light from an excimer-pumped dye module. Neutral density filters were used to ensure the kinetic results did not depend on the dye laser fluence. The laser light from the photolysis laser and dye module counterpropagated through the chamber. Interference filters were used to isolate the LIF signals. The Mo states[4] and corresponding LIF transitions[5] are given in Table 1. A photomultiplier tube was used in collecting the LIF which was subsequently sent to a gated boxcar sampling module, and the digitized output was stored and analyzed by a computer.

The molybdenum precursor was entrained in a flow of buffer gas (Ar or N_2). The diluted molybdenum precursor, buffer gas, and oxidant flowed through mass flow meters and flow controllers prior to admission to the reaction chamber. Total flows were between 150 and 5100 sccm, depending on the total pressure. Pressures were measured with MKS Baratron manometers, and chamber temperatures were measured with a thermocouple.

Reaction time was taken as the delay time between the photolysis pulse and the dye-laser pulse. The delay time was varied by a digital delay generator controlled by a computer. Minimum delay times were typically 1−3 μs in order to avoid any prompt emission from photofragments. The trigger source for these experiments was scattered pump laser light incident upon a fast photodiode. LIF decay traces consisted of 200−500 points, each point averaged over 2−10 laser shots. LIF intensities were proportional to Mo number densities.

Reagents. The following reagents were used as received: $Mo(CO)_6$ (Johnson Matthey, 99%), $MoCl_4$ (Aldrich, 90%), Ar (Potomac Airgas, Inc., 99.998%), N_2 (Potomac Airgas, Inc., 99.998%), SO_2 (MG Industries, 99.98%), CO_2 (MG Industries, anaerobic grade, 99.9%), N_2O (Union Carbide, 99.0%), NO (Liquid Carbonic, 99.0%). $MoCl_4$ was used exclusively at temperatures above ≈540 K due to decomposition of $Mo(CO)_6$ at temperatures above 540 K. Although we used $MoCl_4$ in a few experiments below 540 K, $Mo(CO)_6$ was the precursor of choice because it has a higher vapor pressure than $MoCl_4$. Below 540 K, measured rate constants were independent of the Mo source.

Data Analysis and Results

Experiments were typically performed at 20 Torr total pressure using argon bath gas at room temperature. Experiments were performed in the temperature range 295−621 K. Precursor partial pressures were ≈0.1−0.5 mTorr, and oxidant partial pressures were usually less than a fraction of a percent of the total pressure. Because energy-transfer processes and observable consecutive-type depletion kinetics were found to be important in these Mo/OX systems, rate constants were also measured in N_2 bath gas at a total pressure of 10 Torr. We were unable to obtain an adequate signal-to-noise ratio, S/N, for the excited states of Mo at higher total pressures using N_2 buffer. Additionally, the lifetimes of these states decreased with increasing N_2 pressures such that 10 Torr was the maximum pressure that could be used to obtain accurate rate constants.

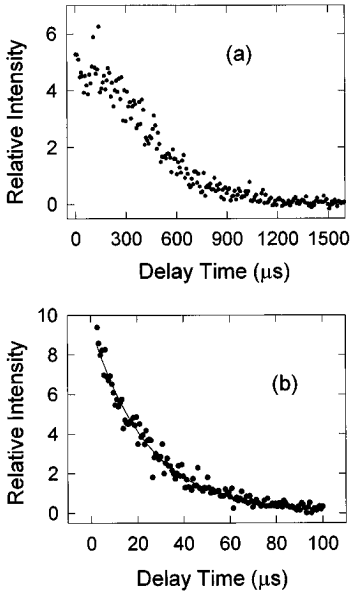

Figure 1. Production and decay of Mo(a^5D_0) following the 248 nm photodissociation of $Mo(CO)_6$ in Ar buffer. T = 296 K, P_{tot} = 20 Torr, [$Mo(CO)_6$] ≈ 0.2 m Torr, and laser fluence ≈ 60 mJ/cm^2. (a) No added OX. (b) 32.2 mTorr of NO; solid line is an exponential fit with τ = 26.6 μs.

Following photodissociation of $Mo(CO)_6$ in argon buffer, in the absence of oxidant, significant growth was observed for all states investigated. This growth is exhibited in Figure 1a for Mo(a^5D_0). The growth is attributed to collisional quenching of higher lying excited states and dissociation of photofragments. We detected excited Mo states up to 16 800 cm^{-1} (a^5G_J) (these states decayed exponentially under all conditions—with and without added O_2).[1] Other workers have studied the 248 nm photodissociation of $Mo(CO)_6$ and have observed emission from Mo states lying as high as 31 655 cm^{-1} for fluences >10 mJ cm^{-2}, indicating a multiphoton (>3 photons) process.[10] Their results and energetic considerations indicate that ground state Mo is formed via a two-photon process, and the excited states are produced by a three-photon process. Thus, the production of Mo states up to ≈36 000 cm^{-1} is energetically possible. Addition of oxidant (NO, in this case) eliminates the growth as shown in Figure 1b; the solid line through the data is an exponential fit to the equation

$$I = I_0 \exp(-t/\tau) \qquad (1)$$

where I and I_0 are the LIF signals at time t and time 0, respectively, and τ is the lifetime from which the pseudo-first-order rate constant, $1/\tau$, is obtained. The fit is from a delay of 1.0 μs and extends for ≈4 lifetimes. The reproducibility of our measured τ's is ± 10% for single-exponential decays and ±25% for biexponential decays (discussed below). Conditions were always chosen so that growth processes were unimportant in obtaining rate constants, i.e., we ensured τ did not depend on photolysis and dye-laser fluence, precursor partial pressure, and total flow rate. We previously reported a kinetic study on Mo + O_2 using this identical experimental method.[1] Our measured rate constant for Mo(a^7S_3) + O_2 agrees with that obtained using a flow tube/laser vaporization technique,[9] indicating growth processes were not important. The growth

diminished with increasing total pressures. The use of $MoCl_4$ without added oxidant also resulted in growth at short times; however, the growth was not as pronounced. Growth at short times was virtually nonexistent when using N_2 buffer. The absence of growth is attributed to the collisional relaxation of photofragments that ultimately dissociate to produce Mo atoms and to the quenching of higher energy states of Mo. $1/\tau$ is given by the expression

$$1/\tau = 1/\tau_0 + k[\mathrm{OX}] \qquad (2)$$

where k is the second-order rate constant, [OX] is the number density of OX, and τ_0 is the lifetime of Mo without added OX. τ_0 represents the lifetime of Mo in the presence of other species in the reaction chamber and diffusion out of the detection zone; τ_0 is usually large compared to the lifetimes with added OX. Second-order rate constants are determined from plots of $1/\tau$ versus oxidant partial pressure such as that shown in Figure 2. The slope yields the observed bimolecular rate constant, k. Such plots typically extend over a 10-fold partial pressure (of OX) range. Experiments described here were repeated at different total pressures and temperatures, depending on the system.

Since the decay kinetics of Mo with OX were also investigated in N_2, we first present quenching (physical) results due to N_2 as these results are instrumental in interpreting the decay kinetics of Mo + OX in N_2 buffer.

Quenching by N_2. Single-exponential temporal behavior was not observed for Mo(a^5S_2) and Mo(a^5D_0) in the presence of added N_2, as observed in Figure 3a for Mo(a^5D_0). Thus, a similar decay scheme is indicated for both states. Under these conditions, a relatively fast decay rate of Mo(a^5D_0) is observed at times less than ≈50 μs, and a slower decay rate is observed at longer times. The decay rates of both portions of the decay trace depend on added N_2. Thus, we attribute this behavior to the collisional deactivation of a higher energy state to Mo(a^5D_0). The solid line through the experimental points in curve a is a biexponential fit. The fit assumes a kinetic model of the form

$$\mathrm{Mo}(a^5D_0) + N_2 \rightarrow \mathrm{Mo}' + N_2 \qquad k_{\mathrm{fast}} \qquad (3)$$

$$\mathrm{Mo}'' + N_2 \rightarrow \mathrm{Mo}(a^5D_0) + N_2 \qquad k_{\mathrm{slow}} \qquad (4)$$

where Mo′ and Mo″ are states lower and higher in energy, respectively, than the a^5D_0 state. The rate equations for reactions 3 and 4 can be solved to yield the biexponential expression

$$[a^5D_0] = A_1 \exp(-t/\tau_1) + A_2 \exp(-t/\tau_2) \qquad (5)$$

$$A_1 = [a^5D_0]_0 - [\mathrm{Mo}'']_0 k_{\mathrm{slow}}/(k_{\mathrm{fast}} - k_{\mathrm{slow}}) \qquad (5a)$$

$$A_2 = [\mathrm{Mo}'']_0 k_{\mathrm{slow}}/(k_{\mathrm{fast}} - k_{\mathrm{slow}}) \qquad (5b)$$

where [ ]$_0$ indicates initial number densities. τ_1 and τ_2 are determined by a fit of the decay profile using a nonlinear fitting routine. k_{fast} and k_{slow} are determined from plots of $1/\tau_1$ vs P_{N_2} and $1/\tau_2$ vs P_{N_2}, respectively, as shown in Figure 3b. For N_2 pressures greater than ≈0.8 Torr, τ_1 was too short to obtain meaningful k_{fast} values. In fact, the rapid decay observed in Figure 3a is virtually nonexistent at N_2 pressures above ≈1 Torr, and only the long time behavior is observed. The model represented by reactions 3 and 4 is oversimplified. Although written as a two-step mechanism, it could involve three or more steps with k_{slow} being a weighted average of the respective rate constants. Biexponential behavior is still predicted for Mo″ + N_2 having additional exit channels.[11] We estimate the overall uncertainty[1] in k_{fast} and k_{slow} to within ±50%. It is worth mentioning that the long time temporal behavior observed in Figure 3a is independently exponential over 3−4 lifetimes (a log I versus t plot yields the same τ_2, to within experimental error). The $J = 1-4$ spin−orbit states of the a^5D_J term decayed exponentially with added N_2, although some of them exhibited a minor growth for 1−3 μs following the photolysis pulse.

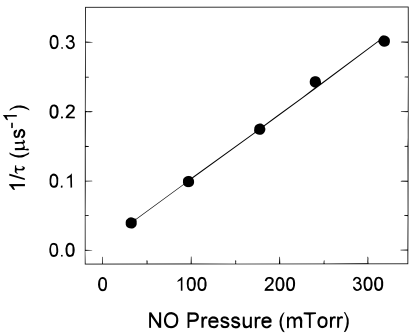

Figure 2. Typical plot for determining second-order rate constants. Conditions are the same as for Figure 1. The slope yields $k = (2.9 \pm 0.8) \times 10^{-11}$ cm^3 s^{-1}.

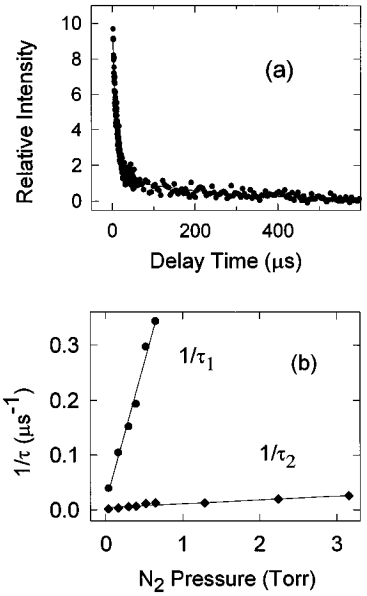

Figure 3. Collisional disappearance of Mo(a^5D_0) by N_2. $T = 295$ K, $P_{\mathrm{tot}} = 20$ Torr (Ar buffer), precursor = $Mo(CO)_6$. (a) Biexponential decay plot for 163 mTorr of added N_2; solid line is a biexponential fit with $\tau_1 = 9.27$ μs, $\tau_2 = 249$ μs. (b) Determination of the second-order rate constants. See text for results of fit.

TABLE 2: Measured Second-Order Rate Constants for the Collisional Disappearance of Mo(a^5S_2,a^5D_J) by N_2 in Ar Buffer[a]

		k's (10^{-12} cm^3 s^{-1})		
Mo state	T (K)	k_{fast}	k_{slow}	k_{true}[b]
a^5S_2	296	23 ± 7	0.18 ± 0.09	23 ± 7
	455	[c]	0.46 ± 0.23	[c]
a^5D_0	296	16 ± 8	0.21 ± 0.11	16 ± 8
a^5D_{1-4}	296			0.13 ± 0.04
	455			0.40 ± 0.12

[a] Total pressure = 20−50 Torr. [b] k_{true} = rate constant for the depletion of the state in question. [c] Did not attempt to measure.

Rate constants for the Mo/N_2 system are summarized in Table 2. The listed k_{true} values are the rate constants for the *depletion* of the states in question. Note the relatively large value of $k(a^5S_2)$. In 10 Torr of neat N_2 buffer, Mo(a^5S_2) has virtually decayed away in less than 1 μs; therefore, the temporal behavior of Mo(a^5S_2) in neat N_2 buffer represents the decay rates of higher

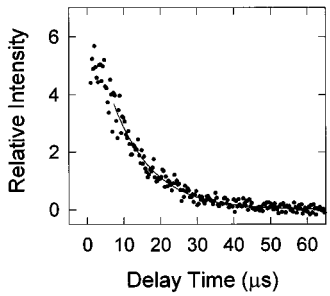

Figure 4. Mo(a^7S_3) + SO_2. T = 295 K, P_{tot} = 40 Torr (Ar buffer), precursor = $MoCl_4$, 15.7 mTorr SO_2; solid line is an exponential fit with τ = 10.4 μs.

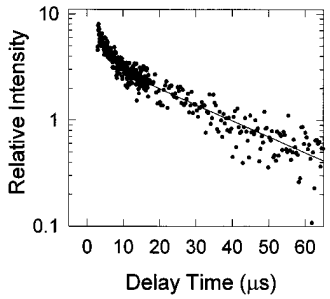

Figure 5. Mo(a^5D_0) + SO_2. T = 296 K, P_{tot} = 40 Torr (Ar buffer), precursor = $Mo(CO)_6$, 4.64 mTorr SO_2; solid line is a biexponential fit with τ_1 = 2.89 μs, τ_2 = 28.7 μs.

energy state(s). The rate constants for the a^5D_{1-4} spin−orbit states are identical, to within experimental uncertainty, and have a value of (1.3 ± 0.4) × 10^{-13} cm^3 s^{-1} at room temperature. The large rate constant at 455 K gives an activation energy of ≈1.9 kcal/mol and an A factor of ≈3.2 × 10^{-12} cm^3 s^{-1}.

Mo + SO_2. Figure 4 shows a decay profile for the reaction of Mo(a^7S_3) with SO_2 using the precursor $MoCl_4$. Note the growth at $t \approx 1-7$ μs. The exponential fit is from 8 to 60 μs. This growth was observed under all conditions, using both $MoCl_4$ and $Mo(CO)_6$. We attribute the growth to thermalization of photofragments and the decay of excited states of molybdenum, Mo*, to ground state Mo via collisions with SO_2. (The growth exhibited at short times in Figure 4 was also observed in some of the other Mo + OX systems studied here and will be noted where applicable.)

The decays of Mo(a^5S_2) in the presence of SO_2 was, for the most part, exponential, with a small tail presenting itself after ≈90% decay in Ar buffer. The small tail might be due to the collisional deactivation of a higher energy state to Mo(a^5S_2). k(a^5S_2) is (3.8 ± 1.9) × 10^{-10} cm^3 s^{-1} in Ar, but in N_2 it is (1.7 ± 0.5) × 10^{-10} cm^3 s^{-1}. As noted above in the N_2 section, the depletion kinetics of Mo(a^5S_2) in N_2 buffer is due to another Mo state. Therefore, the actual rate constant, k_{true}, is k_{fast}.

We are unable to report a "true" depletion rate constant for Mo(a^5D_0) + SO_2 because the decay rates in Ar buffer were too rapid at relatively short times, and the intensity of the slower decay portion of the decay trace accounted for as much as 70−90% of the total LIF intensity, depending on conditions. This short-time nonexponential behavior is shown in Figure 5. The long-time temporal behavior is exponential. We were unable to measure depletion rates of Mo(a^5D_0) + SO_2 in N_2 buffer because of a low S/N. Mo(a^5D_{1-4}) decay profiles exhibited exponential behavior and thus were fitted using eq 1 in the form log I *vs* time. The measured second-order rate constants for the reactions of Mo with SO_2 are all on the order of the gas kinetic rate constant (≈2 × 10^{-10} cm^3 s^{-1}) as seen in Table 3. (In this table and all subsequent tables, k_{fast} and k_{slow} represent measured biexponential rate constants in Ar buffer for the Mo + OX interaction in question.) Identical rate constants using both Ar and N_2 buffers are observed for J = 1−4 of the a^5D_J term. On the basis of our measured rate constants of the other states of Mo interacting with SO_2, we estimate k(a^5D_0) ≈ 3 × 10^{-10} cm^3 s^{-1}.

TABLE 3: Measured Second-Order Rate Constants for the Collisional Disappearance of Mo(a^7S_3,a^5S_2,a^5D_J) by SO_2 at 297 K[a]

	k's (10^{-10} cm^3 s^{-1})			
Mo state	k_{fast}	k_{slow}	k(in N_2)	k_{true}
a^7S_3	1.3 ± 0.3			1.3 ± 0.3[b]
a^5S_2	3.8 ± 1.9	[c]	1.7 ± 0.5	3.8 ± 1.9
a^5D_0	[d]	2.2 ± 0.8		[d]
a^5D_{1-4}	1.8 ± 0.9		1.8 ± 0.6	1.8 ± 0.6

[a] P_{tot} = 10−40 Torr in Ar and 10 Torr in N_2. k_{fast} and k_{slow} are measured biexponential rate constants in Ar buffer. States without a k_{slow} decayed exponentially in Ar buffer. [b] P_{tot}(in Ar) = 10−200 Torr. [c] A small tail whose temporal behavior appeared to depend on the SO_2 partial pressure. We were unable to obtain consistent lifetimes due to low S/N. [d] Unable to measure and therefore could not determine k_{true}. See text.

Mo + CO_2. Ground state Mo is unreactive toward CO_2. We report an upper limit of k = 10^{-15} cm^3 s^{-1}. We attempted to measure rate constants for this reaction over the temperature range 296−621 K and over the total pressure range 100−600 Torr using argon buffer. The room temperature rate constant is probably much less than 10^{-15} cm^3 s^{-1} since the activation energy for this reaction over our temperature range is probably large. Akhmadov et al. measured an activation energy of 19.5 kcal mol^{-1} using a shock wave technique.[8] With such a large activation energy, we would not be able to measure a depletion rate, even at 621 K, the maximum attainable temperature of our oven. Lian et al.[9] reported the value k = 5.3 × 10^{-14} (±30%), which is 50 times larger than our upper limit. Since k for the reaction of Mo(a^7S_3) with O_2 is near the gas kinetic rate,[1,9] an impurity level of 500 ppm O_2 would result in a rate constant near the value reported by Lian et al. When we used anaerobic grade CO_2 (<10 ppm O_2), we did not observe any decay due to CO_2. However, we did observe some decay using standard grade CO_2. It is possible that their larger value is due to impurities. Nevertheless, both these studies show that Mo(a^7S_3) is unreactive toward CO_2.

The decay kinetics of the excited states of Mo in the presence of CO_2 are quite complex. In Ar buffer, biexponential decay kinetics were observed for Mo(a^5S_2) and Mo(a^5D_0). Single-exponential decay kinetics in Ar were observed only for Mo(a^5D_4). In Ar, the a^5D_1 and a^5D_3 states were, for the most part, exponential, with a small tail that became evident after ≈80% decay. The temporal dependence of the tails appeared to depend on the CO_2 partial pressure, but we were unable to obtain consistent lifetimes due to low signal-to-noise ratios. Mo(a^5D_2) had a rapid decay at relatively short times followed by a longer, exponential decay; we were unable to obtain an accurate measure of k_{fast} for this reaction. The depletion kinetics were also measured in N_2 buffer. We were able to obtain rate constants for only Mo(a^5S_2) and two states in the a^5D term. The depletion rate constants are listed in Table 4. There appears to be no consistency between the rate constants measured in Ar and N_2 buffer. The kinetics in the Mo/CO_2 system are obviously complex and involve energy-transfer processes and possibly mixing between the states.

Mo + N_2O. Ground state Mo was found to be unreactive toward N_2O at room temperature. Unlike the Mo(a^7S_3)/CO_2 system, observable reaction rates were measured for Mo(a^7S_3) + N_2O as the temperature was increased. The measured rate

TABLE 4: Measured Second-Order Rate Constants for the Collisional Disappearance of Mo(a^7S_3,a^5S_2,a^5D_J) by CO_2 at 297 K[a]

	k's (10^{-12} cm^3 s^{-1})			
Mo state	k_{fast}	k_{slow}	k(in N_2)	k_{true}
a^7S_3				<0.001
a^5S_2	38 ± 19	4.2 ± 1.3	14 ± 4	38 ± 19
a^5D_0	15	3.0 ± 0.9		15
a^5D_1	5.0 ± 1.5	*b*	18 ± 5	*c*
a^5D_2	>5	3.0 ± 0.9	18 ± 5	*c*
a^5D_3	4.0 ± 2.0	*b*	*d*	*c*
a^5D_4	2.9 ± 0.8		*d*	*c*

[a] $P_{tot}(a^7S_3)$ = 100−600 Torr in Ar. P_{tot}(Mo*) = 10−100 Torr in Ar and 10 Torr in N_2. [b] A small tail whose temporal behavior appeared to depend on the CO_2 partial pressure. We were unable to obtain consistent lifetimes due to low S/N. [c] Unable to ascertain actual value of k. See text for discussion. [d] Too complex to adequately fit.

TABLE 5: Measured Second-Order Rate Constants for the Collisional Disappearance of Mo(a^7S_3,a^5S_2,a^5D_J) by N_2O[a]

Mo state	T (K)	k_{true}[b]	k_{slow}	k(in N_2)
a^7S_3	297	$\ll 0.1 \times 10^{-14}$		
	400	0.10×10^{-14}		
	426	0.21×10^{-14}		
	448	0.34×10^{-14}		
	480	0.65×10^{-14}		
	523	1.4×10^{-14}		
	561	3.0×10^{-14}		
	585	4.0×10^{-14}		
	606	5.9×10^{-14}		
	621	6.8×10^{-14}		
a^5S_2	296	25×10^{-11} (fast)	1.3×10^{-11}	0.85×10^{-11}
a^5D_0	296	1×10^{-11} (fast)	0.60×10^{-11}	
a^5D_1	297	0.70×10^{-11}		1.1×10^{-11}
	398	0.77×10^{-11}		
	473	0.96×10^{-11}		
	621	1.3×10^{-11}		
a^5D_2	297	0.84×10^{-11}		0.87×10^{-11}
	398	0.95×10^{-11}		
	472	1.0×10^{-11}		
	621	1.3×10^{-11}		
a^5D_3	296	1.3×10^{-11}		1.3×10^{-11}
	397	1.5×10^{-11}		
	470	1.7×10^{-11}		
	621	2.2×10^{-11}		
a^5D_4	300	0.92×10^{-11}		1.4×10^{-11}
	398	1.3×10^{-11}		
	473	1.7×10^{-11}		
	621	2.5×10^{-11}		

[a] Units are cm^3 s^{-1}. Uncertainties are ±30% except for a^5S_2(in Ar) and a^5D_0, which are ±50%. $P_{tot}(a^7S_3)$ = 100−600 Torr in Ar. P_{tot}(Mo*) = 10−100 Torr in Ar and 10 Torr in N_2. [b] k_{true} = rate constant for the depletion of the state in question in Ar buffer. States with a k_{slow} decayed biexponentially in Ar buffer with $k_{fast} = k_{true}$.

constants are listed in Table 5 and are plotted in Arrhenius form in Figure 6. Relatively high total pressures were required for the reaction Mo(a^7S_3) + N_2O because relatively high N_2O pressures were needed for any observable decays of ground state Mo atoms. The Arrhenius equation obtained from the weighted fit in Figure 6 is

$$k(a^7S_3) = (2.0 \pm 0.5) \times 10^{-10} \times \exp[-(9.8 \pm 0.3 \text{ kcal mol}^{-1})/RT] \quad \text{cm}^3\ \text{s}^{-1} \quad (6)$$

where the uncertainties represent one standard deviation (precision). We did not observe a significant decay rate at room temperature. Lian et al.[9] also reports no reaction at room temperature. Extrapolation of our results to 298 K gives k(298 K) = 1.3×10^{-17} cm^3 s^{-1}. Akhmadov et al.[8] reported an activation energy of 8.63 ± 6.33 kcal/mol; this value was measured in a shock tube apparatus and is in agreement with our value.

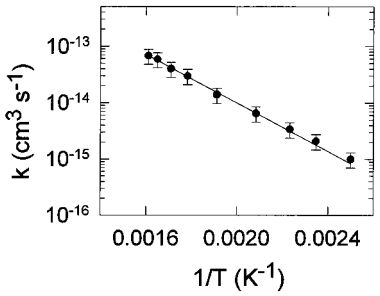

Figure 6. Arrhenius plot for Mo(a^7S_3) + N_2O. P_{tot} = 100−600 Torr (Ar buffer). Solid line is a weighted fit to the expression $k(T) = A \exp(-E_a/RT)$. Error bars represent ±30% uncertainties. See text for results of fit.

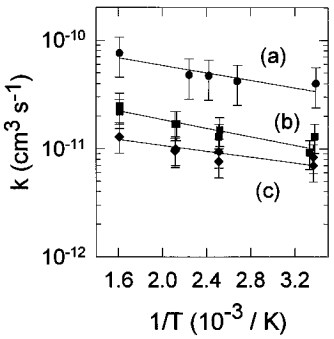

Figure 7. Arrhenius plots at P_{tot} = 20 Torr. (a) Mo(a^5D_4) + NO; (b) Mo($a^5D_{3,4}$) + N_2O; (c) Mo($a^5D_{1,2}$) + N_2O. Error bars represent ±30% uncertainties, except for Mo(a^5D_4) + NO where they are ±40%. Solid lines are weighted fits to the expression $k(T) = A \exp(-E_a/RT)$. See text for results of fits.

The decay kinetics of Mo(a^5S_2) and Mo(a^5D_0) with N_2O were biexponential in Ar buffer while the decay kinetics of the a^5D_{1-4} spin−orbit states were exponential with a little growth at short times (similar to the decay plots involving SO_2 in Figure 4). All states decayed exponentially in N_2 buffer. The rate constants measured in both Ar and N_2 buffer are consistent, as seen in Table 5. k(a^5D_1) in Ar and N_2 appear to be different; however, they are within their combined uncertainties. Mo(a^5D_1) and Mo(a^5D_2) appear to decay at identical rates, to within experimental uncertainty, and so do Mo(a^5D_3) and Mo(a^5D_4). Arrhenius plots for Mo($a^5D_{1,2}$) and Mo($a^5D_{3,4}$) are shown in Figure 7. The rate constants can be expressed as

$$k(a^5D_{1,2}) = (2.0 \pm 0.4) \times 10^{-11} \times \exp[-(0.6 \pm 0.2 \text{ kcal mol}^{-1})/RT] \quad \text{cm}^3\ \text{s}^{-1} \quad (7)$$

$$k(a^5D_{3,4}) = (4.7 \pm 0.8) \times 10^{-11} \times \exp[-(0.9 \pm 0.2 \text{ kcal mol}^{-1})/RT] \quad \text{cm}^3\ \text{s}^{-1} \quad (8)$$

Mo + NO. Variations with total pressure of the second-order rate constants for the reaction of Mo(a^7S_3) with NO are shown in Figure 8, and the rate constants are listed in Table 6. Note that the rate constants increase with increasing total pressure and decreasing temperature. These observations are consistent with a termolecular mechanism. The solid lines through the data in Figure 8 are fits to the simplified falloff expression of Troe[12]

$$\log k = \log\left(\frac{k_0[\text{M}]}{1 + (k_0[\text{M}]/k_\infty)}\right) + \frac{\log F_c}{1 + [\log(k_0[\text{M}]/k_\infty)]^2} \quad (9)$$

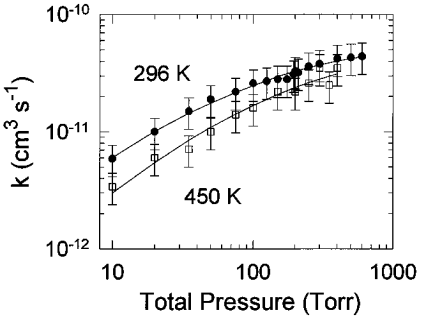

Figure 8. Pressure dependence of the reaction Mo(a^7S_3) + NO at 296 and 450 K. Error bars represent ±30% uncertainties. Solid lines are fits to Troe's falloff expression (see text).

TABLE 6: Measured Second-Order Rate Constants for the Collisional Disappearance of Mo(a^7S_3) by NO in Ar Buffer[a]

T (K)	P_{tot} (Torr)	k (10^{-11} cm^3 s^{-1})	T (K)	P_{tot} (Torr)	k (10^{-11} cm^3 s^{-1})
296	10	0.59	450	10	0.34
	20	1.0		20	0.60
	35	1.5		35	0.71
	50	1.9		50	1.0
	75	2.2		75	1.4
	100	2.7		100	1.6
	125	2.7		150	2.2
	150	2.8		200	2.2
	175	2.8		250	2.6
	195	3.1		300	3.5
	200	3.3		350	2.5
	210	3.2		400	3.5
	250	3.6			
	400	4.2			
	500	4.3			
	600	4.4			
337	20	0.86			
373	20	0.72			
373	200	3.0			
376	20	0.77			
413	20	0.71			
447	200	2.1			
516	20	0.41			
621	20	0.24			

[a] Uncertainties are ±30%.

TABLE 7: Falloff Modeling Parameters for the Reactions of Ti(a^3F_2), Cr(a^7S_3), Fe($^5D_4$), and Mo(a^7S_3) with NO in Ar Buffer

TM	T (K)	k_0 (cm^3 s^{-1})	k_∞ (cm^3 s^{-1})	F_c
Ti[a]	300	$(5.8 \pm 2.6) \times 10^{-31}$	*e*	*e*
Cr[b]	298	$(1.2 \pm 0.2) \times 10^{-30}$	$(3.2 \pm 0.8) \times 10^{-11}$	0.7 (fixed)
Fe[c]	296	2.3×10^{-32}	$\approx 1 \times 10^{-12}$	$\approx$0.7
Mo[d]	296	$(2.6 \pm 0.3) \times 10^{-29}$	$(5.8 \pm 0.5) \times 10^{-11}$	0.72 ± 0.07
Mo[d]	450	$(1.9 \pm 0.3) \times 10^{-29}$	$(7.5 \pm 1.2) \times 10^{-11}$	0.6 (fixed)
		$(1.7 \pm 0.2) \times 10^{-29}$	$(6.0 \pm 0.9) \times 10^{-11}$	0.7 (fixed)
		$(1.7 \pm 0.2) \times 10^{-29}$	$(5.1 \pm 0.7) \times 10^{-11}$	0.8 (fixed)

[a] Reference 14. [b] Reference 13. [c] Reference 15; error estimates not given. [d] This work. [e] Not measured.

where k_0 is the limiting low-pressure third-order rate constant, k_∞ is the limiting high-pressure second-order rate constant, [M] is the buffer gas number density, and F_c is the broadening factor. We obtained large uncertainties in k_∞ and F_c (>100% for F_c) when we fitted eq 9 to the 450 K data. (Not many points are in the falloff region.) Since $F_c = 0.72$ for the 296 K data, as seen in Table 6, we fixed F_c at 0.6, 0.7, and 0.8 to obtain k_0 and k_∞ at 450 K. Values of the parameters in eq 9 are listed in Table 7 and are compared to parameters from other TM/NO complexation systems.[13-15] F_c was fixed at 0.6, 0.7, and 0.8 for Cr + NO because only a small portion of the falloff range was observed;[13] we list only the median value.

TABLE 8: Measured Second-Order Rate Constants for the Collisional Disappearance of Mo(a^5S_2,a^5D_J) by NO[a]

		k's (10^{-11} cm^3 s^{-1})		
Mo state	T (K)	k_{true}	k_{slow}	k(in N_2)
a^5S_2	296	7.2 (fast)	3.3	3.3
	373	*b*	4.2	*b*
	450	*b*	5.3	*b*
a^5D_0	296	3.0		
a^5D_{1-3}	296	3.1		3.9
a^5D_2	374	4.4		*b*
	450	4.9		*b*
a^5D_4	295	3.8		3.8
	373	4.2		*b*
	413	4.7		*b*
	446	4.8		*b*
	621	7.6		*b*

[a] P_{tot} = 10−100 Torr in Ar and 10 Torr in N_2. Uncertainties are ±40% except for a^5S_2 (fast and slow), which are ±50%. States with a k_{slow} decayed biexponentially in Ar buffer with $k_{fast} = k_{true}$. [b] Did not attempt to measure.

The decay kinetics of Mo(a^5S_2) in the presence of added NO were biexponential in Ar buffer and exponential in N_2 buffer. The decay kinetics of the a^5D_J states with NO were all exponential in Ar and N_2. We see in Table 8 that results in Ar and N_2 buffer are consistent. The temperature dependence of $k(a^5D_4)$ is given in Figure 7, and the Arrhenius expression obtained is

$$k(a^5D_4) = (1.3 \pm 0.4) \times 10^{-10} \times \exp[-(0.8 \pm 0.3 \text{ kcal mol}^{-1})/RT] \quad \text{cm}^3\,\text{s}^{-1} \quad (10)$$

The other a^5D_J states are expected to have similar Arrhenius parameters, as seen from *k(T)* for Mo(a^5D_2) in Table 8.

Discussion

The Mo + N_2 and Mo + OX systems are first discussed separately. We then offer general comments about TM depletion kinetics. Because we investigated several atomic states interacting with the oxidants and a proposed model may apply to only one system, we find this order to be a favorable approach in our discussion.

Mo + N_2. Physical quenching is the only exit channel available for excited states of molybdenum interacting with N_2. The vibrational frequency of N_2, $\omega_e(N_2) = 2360$ cm^{-1},[16] is not in resonance with any energy differences, ΔE, between the Mo states,[4] thus making direct E−V,R energy transfer improbable. This implies a collision complex is formed that facilitates the quenching. We omit a detailed discussion on the fate of the quenched Mo species, but several observations stand out that are worth mentioning. The rate constant of Mo(a^5S_2) is significantly larger than the rate constant of the $J = 1-4$ a^5D_J spin−orbit states, but it is only slightly larger than the rate constant of Mo(a^5D_0). The a^5S_2 and a^5D_0 states are 197.64 cm^{-1} apart, and mixing between these states might be induced by collisions with N_2. Identical rate constants for the $J = 1-4$ a^5D_J spin−orbit states indicate either identical rate constants or rapid interconversion among said states under our conditions. Note that $k(a^5D_{1-4}) \approx k_{slow}(a^5D_0) \approx k_{slow}(a^5S_2)$ and that the depletion rate of Mo(a^5S_2) + N_2 in Ar buffer is relatively fast (see Table 2) such that, in neat N_2 buffer, the observed depletion rate of Mo(a^5S_2) in the presence of OX actually represents decay of another state. Also note that in our Mo/OX systems using N_2 buffer $k(a^5S_2) \approx k(a^5D_J)$. These observations indicate that either one or more of the Mo(a^5D_J) spin−orbit states and/or

another Mo state are connected to Mo(a^5D_0) and/or Mo(a^5S_2) via collisions with N_2.

Mo + SO_2. The most likely reaction for ground state Mo is

$$Mo(a^7S_3) + SO_2(X^1A_1) \rightarrow MoO(X^5\Pi_r) + SO(X^3\Sigma^-)$$
$$\Delta H_{298} = -11.0 \text{ kcal/mol}^{17} \quad (11)$$

The large rate constant at 297 K indicates a negligible barrier to reaction. For the Mo* + SO_2 interactions, we cannot unequivocally state that physical quenching is not an important exit channel; two or more exit channels may be operative to varying degrees of importance. It is difficult to rationalize the rate constants for the Mo + SO_2 system in terms of the direct abstraction mechanism since all of the rate constants are large; only the ground state and the a^5S_2 state orbitally correlate with the low-energy MoO states that are energetically accessible.[3] Mo(a^5S_2) + SO_2 has the largest rate constant of the Mo states investigated in the Mo/SO_2 system. Direct physical quenching at such a rapid rate via E−V,R transfer to the ground state is improbable since the ΔE of the Mo states are not in resonance with any vibrational frequencies of SO_2.[18] It is conceivable that its relatively large rate constant is due to a long-range attraction that leads to an entrance channel controlled reaction; i.e., efficient quenching might take place via a charge-transfer intermediate complex. It is also conceivable that the interaction of Mo(a^5D_J) with SO_2 might take place via a charge-transfer complex. Small differences on the potential energy surfaces of Mo($4d^55s^1\ a^5S_2$) and Mo($4d^45s^2\ a^5D_J$) might account for the smaller rate constant of the a^5D_J term; the closed s shell is expected to introduce more electronic repulsive effects. The nonexponential decay plots of Mo(a^5D_0) might be due to physical quenching from higher energy states.

The depletion rates of Mo + SO_2 can be compared to the rates of other SO_2 reactions. The reaction kinetics of ground state Ti with SO_2 is the only other TM/SO_2 system reported.[14] This reaction has an appreciable rate at room temperature: $k = (6.09 \pm 0.95) \times 10^{-11}$ cm^3 s^{-1}. The reaction of B with SO_2[19] proceeds at approximately the collision rate, and the reaction of Ba with SO_2[20−22] has a relatively large reaction cross section. The fast rates of these reactions were attributed to an electron-transfer mechanism (harpooning in the case of Ba). A high-temperature kinetic study of the endothermic reaction of Al with SO_2 has been reported,[23] and reactions of Na[24] and K[25] with SO_2 have been observed to produce stable adducts with k_∞ on the order of the collision rate. Results of these investigations were also explained in terms of an electron-transfer mechanism. On the basis of the limited amount of data on metal atom + SO_2 reactions, it appears that SO_2 is very reactive toward metals. SO_2 has the largest EA of N_2, O_2, and the oxidants in this paper.[26−31]

Mo + CO_2. Ground state Mo is unreactive toward CO_2 under the conditions of our experiments despite the reaction's large exothermicity of 15.5 kcal/mol.[17] The presence of a $d^{n-1}\ s^1$ electron configuration is clearly not a sufficient condition for chemical reactivity. Thus, the direct abstraction mechanism, as defined, cannot account for this observation. This lack of reactivity might be due to the reaction

$$Mo(a^7S_3) + CO_2(X^1\Sigma_g^+) \rightarrow MoO(X^5\Pi_r) + CO(X^1\Sigma^+)$$
$$\Delta H_{298} = -15.5 \text{ kcal/mol}^{17} \quad (12)$$

being spin forbidden. Without knowledge of the potential energy surface and another viable approach, we can only speculate about the production of spin-forbidden states being cause for the lack of reactivity.

Our results indicate that significant energy-transfer processes and mixing are important for the Mo* + CO_2 interactions. The rate constant at 297 K for Mo($4d^55s^1\ a^5S_2$) + CO_2 is relatively large and is expected to be larger than the depletion rate constant of the $4d^45s^2\ a^5D_J$ term on account of the closed s shell in the a^5D_J term. The depletion rates of the excited states are not (solely, if at all) driven by an electron-transfer mechanism since IP(a^5S_2) > IP(a^5D_J) and $k(a^5S_2) \gg k(a^5D_J)$. As seen from the measured rate constants in Table 4, the kinetics in this system are too complex to draw any definitive conclusions.

Mo + N_2O. Results for the reaction Mo(a^7S_3) + N_2O are consistent with a bimolecular reaction. Thus, the most likely reaction channel is

$$Mo(a^7S_3) + N_2O(X^1\Sigma^+) \rightarrow MoO(X^5\Pi_r) + N_2(^1\Sigma_g^+)$$
$$\Delta H_{298} = -103 \text{ kcal/mol}^{17} \quad (13)$$

The relatively large activation energy of 9.8 kcal/mol may be due to the reaction being spin forbidden, as explained above for CO_2. The excited electronic states of MoO that are energetically feasible for this reaction are also quintets,[3] thus making their production spin forbidden. The simple direct abstraction mechanism, which only considers the conservation of orbital occupancy, would predict a small or zero activation energy.

The semiempirical, resonance interaction model uses the modified Arrhenius equation $k(T) = AT^{1/2} \exp(-E/RT)$ in determining the Arrhenius parameters.[7] Using this equation, we obtain the result

$$k(T) = (5.2 \pm 1.1) \times 10^{-12} T^{1/2} \times \exp[-(9.3 \pm 0.2 \text{ kcal mol}^{-1})/RT] \quad \text{cm}^3\ \text{s}^{-1} \quad (14)$$

for Mo(a^7S_3) + N_2O. Our activation energy does not agree with the model's predicted value of 6.72 kcal mol^{-1}. The model assumes that one of the resonance structures has a metal bonding orbital of s character. Although the activated complex structure for the reaction is not known, chemical bonding in MoO involves the d orbitals, and the low-energy states of MoO have a single electron in the 12σ molecular orbital which is nonbonding and primarily centered on Mo.[3] The 12σ molecular orbital is of Mo 5s character and has significant mixing with the Mo 5p orbital. Assuming the conservation of orbital occupancy along the reaction coordinate, the poor agreement between our measured value and the predicted value may be in the model's neglect of the TM's d electrons and of the electronic states of the products formed.

The 298 K rate constants for the ground state reactions of Cr[13,32] and W,[33] which also lie in group 6, with N_2O have also been measured: $k_{Cr} = (1.0 \pm 0.1) \times 10^{-14}$ and $k_W = 2.9 \times 10^{-15}$ (±30%) cm^3 s^{-1}. The resonance interaction model predicts $k_W < k_{Mo} < k_{Cr}$. However, with the extrapolated $k_{Mo} = 1.3 \times 10^{-17}$ cm^3 s^{-1}, we see that the resonance model does not predict the correct ordering of the rate constants ($k_{Mo} < k_W < k_{Cr}$) based on the sum of IP and s−p PE.[7] The electron-transfer mechanism has also been applied to reactions involving TM atoms and OX. For a given OX, a TM atom having a smaller IP than other TMs is expected to exhibit faster reaction rates. The IPs of Cr, Mo, and W are 6.77, 7.10, and 7.98 eV, respectively.[4] Clearly, the electron-transfer mechanism does not explain the rate constant ordering of group 6 TM + N_2O reactions. Thus, the production of spin-forbidden states seems to be the major constraint to the Mo + N_2O reaction.

Mo(a^5S_2) interacts with N_2O at the collision rate. The chemical reaction

$$Mo(a^5S_2) + N_2O(X^1\Sigma^+) \rightarrow MoO(X^5\Pi_r) + N_2(^1\Sigma_g^+) \quad (15)$$

in which Mo(a^5S_2) orbitally correlates with MoO($X^5\Pi_r$), may be operative. Direct E−V,R energy transfer is improbable since no vibrational frequencies of N_2O[18] and $\Delta E(a^5S_2-a^7S_3)$ are in resonance. The depletion of Mo(a^5S_2) might be a direct O atom abstraction taking place on an attractive, excited state surface, unlike the ground state surface where a barrier is encountered. The depletion rate of Mo(a^5S_2) is at least 19 times the depletion rates of the a^5D_J states. The reaction of Mo(a^5D_J) with N_2O to produce ground state MoO would be slower than reaction 15 (as observed) according to the proposed direct abstraction mechanism[2] since the a^5D_J term has a $4d^45s^2$ electron configuration. Although we cannot identify the exit channels for Mo(a^5D_J), our results indicate some energy transfer is occurring. The small activation energies (≈1 kcal/mol or less) measured for Mo(a^5D_J) + N_2O indicate a loose transition state and negligible barriers along the surfaces connecting reactants and products.

Mo + NO. Results of the reaction Mo(a^7S_3) + NO indicate a termolecular reaction mechanism. Production of MoO from this reaction is not thermodynamically feasible under our experimental conditions at 298 K as it is endothermic by 8.2 kcal/mol at 298 K.[17] As seen in Table 7, k_0 is an order of magnitude larger than k_0 for Cr (+NO), which lies above Mo in the periodic table (CrO formation is also endothermic at 298 K).[17] The value of k_∞ for Mo indicates a small barrier to adduct formation. Accurate RRKM[34] calculations could not be performed because interaction potentials, well depths, vibrational frequencies, etc., of MoNO are not known. However, the rather large value of k_0 indicates a higher Mo−NO binding energy (>20 kcal/mol) than Cr−NO. For the Ti/NO system, TiO formation is the dominant channel.[14] However, adduct formation was indicated at room temperature. The reaction was in its third-order kinetic regime up to 200 Torr, the maximum total pressure at which the reactions were studied.

Interestingly, k_0 for Cr and Mo, which have $d^{n-1}s^1$ configurations, are larger than k_0 for Ti and Fe, which have $d^{n-2}s^2$ configurations. In the s^1 configuration, the singly occupied orbital of the TM might overlap favorably with the single electron of NO, forming a bond. This argument has been used to explain the dioxygen complexes of the 3d TM atoms.[35] The 3d work has shown that TMs having a $d^{n-1}s^1$ electron configuration react faster than those with a $d^{n-2}s^2$ configuration. Even if the d electrons of the TM atom were involved in the bonding, the reactivity of the s^2 configuration would still be expected to be less than that of the s^1 configuration because of its diffuse nature. It would be interesting to perform a similar study on TM + NO systems to test the effect of the atomic electron configuration.

Though an extensive investigation into the relative efficiencies of different quenchers was not undertaken, removal rate constants of Mo(a^7S_3) + NO using He, N_2, and SF_6 buffers were measured at a total pressure of 20 Torr. The rate constants $k_{He} < k_{Ar} < k_{N_2} < k_{SF_6}$ follow the trend of larger and/or more complex molecules being more efficient energy stabilizers.

Energetically, the excited states of Mo can react with NO to produce ground state MoO. However, as with the other Mo + OX systems, we cannot distinguish between chemical and physical quenching for any of the excited states. There is some energy transfer occurring by virtue of the biexponential decay kinetics of Mo(a^5S_2). Another indication of physical quenching is the slight nonexponential temporal behavior at relatively short times (similar to the decay plots involving SO_2 in Figure 4) for Mo(a^7S_3) + NO.

General Comments. The oxidants CO_2 and N_2O appear unique among the oxidants studied here. Both are linear, closed-shell molecules; their reactions with ground state Mo are spin-forbidden but exothermic, and they have very small electron affinities (negative in the case of CO_2),[27,29] yet N_2O has an observable reaction rate with ground state Mo while CO_2 does not. Reaction 13 has a significantly larger exothermicity than reaction 12; however, previous studies on other TM/OX systems show no correlation between reaction efficiency and enthalpy of reaction.[14,36,37] For the V + CO_2, N_2O[36,37] and Ti + CO_2, N_2O[14,37] reactions, rate constants for the N_2O reactions are only slightly larger than those for the CO_2 reactions. Although CO_2 and N_2O do not correlate with their ground state fragments, their reactions with V and Ti are spin-allowed. This may explain why the rate constants for the V and Ti reactions are significantly larger than those for the Mo + CO_2, N_2O reactions. SO_2 is also a closed-shell molecule. However, it has a significantly larger EA[31] than CO_2[27] and N_2O,[29] which seems to have a favorable effect on its reactivity with metal atoms.

We now turn our attention to the electron-transfer mechanism. The electron affinities of colliders studied in this work fall in the order EA(N_2) < EA(CO_2) < EA(NO) < EA(N_2O) < EA(O_2) < EA(SO_2).[26−31] The electron-transfer mechanism correctly predicts for the bimolecular reactions of Mo(a^7S_3) with CO_2, N_2O, O_2, and SO_2 that $k(CO_2) < k(N_2O) < k(O_2) < k(SO_2)$ at 298 K, but it is inconsistent with the depletion rates of Mo(a^5S_2) with all of the colliders mentioned above. (Valence interactions are expected to be more important for reactions involving N_2, CO_2, and N_2O on account of their small EAs which cause relatively short curve crossings (within the hard-sphere collision diameter); therefore, the concept of electron transfer in N_2, CO_2, N_2O + TM reactions, especially when the TM has a high IP, may not be valid). The electron-transfer mechanism is also inconsistent with the reaction rates of several oxidants with a given TM atom (Sc, Ti, V).[14,36,37] It accounts for the ordering of the rate constants of the 3d TM atoms Sc, Ti, and V with a given oxidant[37] but fails when the 4d and 5d TM atoms Mo[1] and W[2] are included. This mechanism is also inconsistent with the depletion rates of Mo (including Mo*) with O_2[1] and the oxidants studied here. Higher energy states should deplete at a faster rate since they effectively have lower IPs. We find that the $4d^55s^1$ a^5S_2 state, which is the lowest energy excited state of Mo, depletes faster than the $4d^45s^2$ a^5D_J term in the presence of the oxidants, lending support for the importance of electron configurations in the depletion kinetics of TMs. In the case of Mo + O_2, the $4d^55s^1$ a^7S_3 ground state also depletes faster than the a^5D_J term, which has over 10 000 cm^{-1} more electronic energy. Thus, even though some charge transfer might be operative to some extent, as discussed above for the SO_2 reactions, there are shortcomings to the electron-transfer mechanism in explaining the reactivity of TM atoms. Fast reactions such as alkali metal atoms + halogen molecules can be satisfactorily explained by the harpoon mechanism; the alkali metal atoms have relatively small IPs, and the halogen molecules have relatively large EAs. Thus, such reactions are entrance-controlled. The reactions of TM atoms with oxidants (those studied here) are expected to experience valence interactions since the IPs of the TM atoms are relatively large, and the EAs of the oxidants are generally smaller than those of the halogens.

It has been shown here and elsewhere[2,35] that the electronic structure of TM atoms plays a role in their depletion kinetics. States (ground and excited) evolving from a $d^{n-1}s^1$ electron configuration deplete faster than those evolving from a $d^{n-2}s^2$

electron configuration in many cases. The diffuse, closed s subshell in the s^2 configuration causes electronic repulsive effects, thus reducing the reactivity. Additionally, the $d^{n-1}s^1$ electron configuration in some of the TM atoms orbitally correlate with their low-energy TM monoxides and (probably) causes the enhanced reactivity relative to the $d^{n-2}s^2$ states. Such kinetic results have been observed for bimolecular as well as association reactions. Our results generally follow along this same pattern. However, other factors such as the electronic structure of the oxidant and product states appear important, as indicated above for the Mo(a^7S_3) + CO_2 and N_2O reactions.

Summary and Conclusions

Our results indicate reaction and energy-transfer processes for the collisional disappearance of Mo(a^7S_3), Mo(a^5S_2), and Mo(a^5D_J) by N_2, SO_2, CO_2, N_2O, and NO. Bimolecular reaction kinetics are observed for the reactions of Mo(a^7S_3) with SO_2 and N_2O, termolecular reaction kinetics with NO, and no reactions with CO_2. The $4d^55s^1$ a^5S_2 excited state depletes faster than the higher energy $4d^45s^2$ a^5D_J term in all cases. Rate efficiencies do not appear to depend entirely on the electron configuration of Mo, nor entirely on the propensity for electron transfer, as observed in other works.[1,2,14] The resonance interaction model is inconsistent in explaining the rate constants for the reactions of Mo (and Cr and W) with N_2O. A comparison of our results with other TM systems indicates that atomic structure (in particular, the $d^{n-1}s^1$ configuration) is a driving force in the *depletion* kinetics and that the production of spin-forbidden states might be responsible for reduced reactivities. State-to-state dynamic studies and theoretical investigations on TM + OX systems would cast further light on possible TM oxidation mechanisms.

Acknowledgment. This research was supported by the Naval Academy Research Council, the Office of Naval Research, and a Cottrell College Science Award of Research Corporation.

References and Notes

(1) Campbell, M. L.; McClean, R. E.; Harter, J. S. S. *Chem. Phys. Lett.* **1995**, *235*, 497.
(2) Campbell, M. L.; McClean, R. E. *J. Chem. Soc., Faraday Trans.* **1995**, *91*, 3787 and references therein.
(3) Hamrick, Y. M.; Taylor, S.; Morse, M. D. *J. Mol. Spectrosc.* **1991**, *146*, 274.
(4) Moore, C. E. *Atomic Energy Level as Derived from the Analysis of Optical Spectra*; *Natl. Stand. Ref. Data Ser. (U.S. Natl. Bur. Stand.)* **1971**, *NSRDS-NBS 35*.
(5) Whaling, W.; Hanaford, P.; Lowe, R. M.; Biemont, E.; Grevesse, N. *J. Quant. Spectrosc. Radiat. Transfer* **1984**, *32*, 69.
(6) Herschbach, D. R. *Adv. Chem. Phys.* **1966**, *10*, 319.
(7) Futerko, P. M.; Fontijn, A. *J. Chem. Phys.* **1991**, *95*, 8065.
(8) (a) Akhmadov, U. S.; Zaslonko, I. S.; Smirnov, V. N. *Kinet. Catal.* **1988**, *29*, 251. (b) Akhmadov, U. S.; Zaslonko, I. S.; Smirnov, V. N. *Kinet. Catal.* **1988**, *29*, 808.
(9) Lian, L.; Mitchell, S. A.; Rayner, D. M. *J. Phys. Chem.* **1994**, *98*, 11637.
(10) Tyndall, G. W.; Jackson, R. L. *J. Phys. Chem.* **1991**, *95*, 687 and references therein.
(11) The rate equations can be solved to yield biexponential expressions for Mo(a^5D_0) or any other Mo state that undergoes a similar reaction scheme; see ref 1. Additionally, modeling computations were performed on the decay schemes presented in this paper using a "Kinetics Integration Package from ARSoftware". The qualitative features of the nonexponential decay plots were reproduced. The computations are, at best, semiquantitative, because the initial number densities of the formed Mo atoms were not determined.
(12) Troe, J. *J. Phys. Chem.* **1979**, *83*, 114.
(13) Parnis, J. M.; Mitchell, S. A.; Hackett, P. A. *J. Phys. Chem.* **1990**, *94*, 8152.
(14) Campbell, M. L.; McClean, R. E. *J. Phys. Chem.* **1993**, *97*, 7942.
(15) Mitchell, S. A.; Hackett, P. A. *J. Chem. Phys.* **1990**, *93*, 7822.
(16) Herzberg, G. *Molecular Spectra and Molecular Structure I, Spectra of Diatomic Molecules*, 2nd ed.; Van Nostrand: Princeton, 1950.
(17) Chase, M. W., Jr., Davies, C. A., Downey, J. R., Jr., Frurip, D. J., McDonald, R. A., Syverud, A. N., Eds. *JANAF Thermochemical Tables*, 3rd ed.; *J. Phys. Chem. Ref. Data* **1985**, *14* (Suppl. 1).
(18) Herzberg, G. *Molecular Spectra and Molecular Structure III, Electronic Spectra and Electronic Structure of Polyatomic Molecules*; Van Nostrand Reinhold: New York, 1966.
(19) DiGiuseppe, T. G.; Davidovits, P. *J. Chem. Phys.* **1981**, *74*, 3287.
(20) Smith, G. P.; Zare, R. N. *J. Am. Chem. Soc.* **1975**, *97*, 1985.
(21) Behrens, R., Jr.; Freedman, A.; Herm, R. R.; Parr, T. P. *J. Am. Chem. Soc.* **1976**, *98*, 294.
(22) Freedman, A.; Parr, T. P.; Behrens, R., Jr.; Herm, R. R. *J. Chem. Phys.* **1979**, *70*, 5251.
(23) Fontijn, A.; Felder, W. *J. Chem. Phys.* **1979**, *71*, 4854.
(24) Shi, Y.; Marshall, P. *J. Phys. Chem.* **1991**, *95*, 1654.
(25) Goumri, A.; Laakso, D.; Rocha, J.-D. R.; Francis, E.; Marshall, P. *J. Phys. Chem.* **1993**, *97*, 5295.
(26) $EA(N_2) = -1.6$ eV: Rosenstock, H. M.; Draxl, K.; Steiner, B. W.; Herron, J. T. *J. Phys. Chem. Ref. Data* **1977**, *6* (Suppl. 1).
(27) $EA(CO_2) = -0.6$ eV: Compton, R. N.; Reinhardt, P. W.; Cooper, C. D. *J. Chem. Phys.* **1975**, *63*, 3821.
(28) $EA(NO) = 0.026$ eV: Travers, M. J.; Cowless, D. C.; Ellison, G. B. *Chem. Phys. Lett.* **1989**, *164*, 449.
(29) $EA(N_2O) = 0.22$ eV: Hopper, D. G.; Wahl, A. C.; Wu, R. L. C.; Tiernan, T. O. *J. Chem. Phys.* **1976**, *65*, 5474.
(30) $EA(O_2) = 0.451$ eV: Travers, M. J.; Cowless, D. C.; Ellison, G. B. *Chem. Phys. Lett.* **1989**, *164*, 449.
(31) $EA(SO)_2 = 1.107$ eV: Nimlos, M. R.; Ellison, G. B. *J. Phys. Chem.* **1986**, *90*, 2574.
(32) Fontijn, A.; Blue, A. S.; Narayan, A. S.; Bajaj, P. N. *Combust. Sci. Technol.* **1994**, *101*, 59.
(33) Harter, J. S. S.; Campbell, M. L.; McClean, R. E. Manuscript in preparation.
(34) Robinson, P. J.; Holbrook, K. A. *Unimolecular Reactions*; Wiley-Interscience: New York, 1972.
(35) Brown, C. E.; Mitchell, S. A.; Hackett, P. A. *J. Phys. Chem.* **1991**, *95*, 1062.
(36) McClean, R. E.; Pasternack, L. *J. Phys. Chem.* **1992**, *96*, 9828.
(37) Ritter, D.; Weisshaar, J. C. *J. Phys. Chem.* **1990**, *94*, 4907.

JP9532172